Materials Today Sustainability 31 (2025) 101172

Contents lists available at ScienceDirect

Materials Today Sustainability

journal homepage: www.journals.elsevier.com/materials-today-sustainability

Unlocking improved hydrogen storage: Thermodynamic tuning and ionic conductivity boost in Fe-doped Mg_2NiH_4

Ikram Belkoufa [a,*], Abdelmajid Assila [a], Seddiq Sebbahi [a,b], Amine Alaoui-Belghiti [a,**], Said Laasri [a,c], Mouhaydine Tlemçani [d], El Kebir Hlil [e], Abdelowahed Hajjaji [a]

[a] Laboratoire des Sciences de l'Ingénieur pour l'Energie, École Nationale des Sciences Appliquées d'El Jadida, BP 1166, Plateau, EL Jadida, 24002, Morocco
[b] Research Institute for Solar Energy and New Energies (IRESEN), Morocco
[c] Polydisciplinary Faculty of Sidi Bennour, Chouaib Doukkali University, El Jadida, Morocco
[d] Department of Mechatronics Engineering, School of Science and Technology, Universidad de Évora, Colégio Luis António Verney, Rua Romão Ramalho, N° 59, 7000–671, Évora, Portugal
[e] Univ. Grenoble Alpes, CNRS, Grenoble INP, Institut Néel, 38000, Grenoble, France

ARTICLE INFO

Keywords:
Mg_2Ni alloys
Fe substitution
Hydrides
First principles
Hydrogen storage
Ionic conductivity
Thermodynamic properties

ABSTRACT

Mg_2Ni is considered a promising candidate for hydrogen storage materials due to its reasonable hydrogenation and dehydrogenation kinetics and cost-effectiveness. However, the high thermodynamic stability of Mg_2NiH_4 poses a significant challenge in terms of the operating temperature required for hydrogen release. This study investigates the crystal and electronic structure, and thermodynamic stability of Iron-doped Mg_2NiH_4 and their alloys using first-principles calculations based on density functional theory. The results demonstrate that by replacing one in sixteen Mg atoms and one in eight Ni atoms with Fe, the enthalpy of hydrogen desorption can be reduced from 65.173 to 57.58 and 50.72 kJ/mol H_2, respectively. Furthermore, the study clarifies the crystal structure and electron properties of Fe-doped Mg_2Ni and Mg_2NiH_4, highlighting the significant role of weakened covalent interactions in the H–Ni bonding that contribute to the reduced thermodynamic stability of the hydrides. This study demonstrates that ionic conductivity improves with the destabilization of Mg_2NiH_4, achieving up to 5×91.10^{-1} S/cm for $Mg_{15}FeNi_8H_{32}$ at 400 K. Substituting magnesium (Mg) with iron (Fe) significantly impacts the electronic structure of the material. The additional d-electrons from Fe enhance the density of electronic states near the Fermi level, leading to increased charge carrier mobility and, consequently, higher conductivity. In contrast, replacing nickel (Ni) with Fe has a less pronounced effect, as both Ni and Fe are transition metals with similar electronic configurations and d-electrons near the Fermi level. This results in fewer new electronic states and a smaller increase in conductivity compared to Mg substitution.

Nomenclature

N_A	Avogadro's number (mol^{-1})
K_B	Boltzmann constant (J/K)
E_a	Activation energy (Joule)
Z	Atomic number
e	Elementary charge
T	Temperature (K)
M	molar mass of the ion (Kg)
n_H	Number of moles of hydrogen absorbed in host material
V	Volume (m^3)
m_H	Mass of hydrogen absorbed in host material (Kg)
l	Short distance between two hydrogen atoms of hydrogen (m)
$\boldsymbol{v}$	Speed (m/s)
$\boldsymbol{\tau_0}$	time constant of the system (s)

1. Introduction

The pursuit of alternative and sustainable energy sources has intensified due to finite energy resources and increasing environmental pollution. Hydrogen, recognized as a clean energy carrier, has garnered

This article is part of a special issue entitled: Sustainable H2 Fuel published in Materials Today Sustainability.

* Corresponding author.
** Corresponding author.
E-mail addresses: belkoufa.i@ucd.ac.ma (I. Belkoufa), alaouibelghiti.a@ucd.ac.ma (A. Alaoui-Belghiti).

https://doi.org/10.1016/j.mtsust.2025.101172
Received 24 December 2024; Received in revised form 15 May 2025; Accepted 27 June 2025
Available online 1 July 2025

significant interest. However, one of the primary obstacles to the realization of a hydrogen economy is efficient hydrogen storage [1,2]. Solid-state hydrogen storage materials, notably lightweight metal hydrides which entrap hydrogen atoms within their crystal structures, have gained significant interest due to their safety and effectiveness attributes [3,4]. Hydrides based on magnesium are one of the most researched groups of materials for solid-state hydrogen storage [1, 5–10]. In the literature, pure magnesium is frequently referred to as "light," although its low crystalline density (1.45 g/cm^3) is an inconvenience since it translates to a non-spectacular volumetric density (110 kg/m^3) of stored hydrogen. In practice, when the apparent density of the powder is considered, it is close to the current AB_5 compounds (90–95 kg/m^3). As compared to magnesium hydride [64], Mg_2Ni-type alloy hydrides remain appealing hydrogen storage materials because to their high hydrogen capacity (3.6 wt%), light weight, and low cost [11–13]. However, due to unfavorable thermodynamics, poor hydrogenation/dehydrogenation kinetics, and the release of unwanted by-products, the alloy materials have not found practical use [14]. Many studies have been conducted to overcome these disadvantages and improve the characteristics of hydrogen storage by modifying the microstructure by mechanical alloying [15] as well as alloying with additional components [16–21]. Numerous efforts have been undertaken to alter the enthalpy of hydrogen desorption through alloy chemistry [22]. One of the notable examples in hydrogen storage is Mg_2NiH_4. This material has the capability to reversibly store 3.6 wt% of hydrogen, which is an improvement over MgH_2, and its sorption kinetics are notably enhanced. However, despite these advantages, its measured hydrogen desorption enthalpy, represented by $\Delta H_{des} = 0.67$ eV/H_2, remains relatively high for practical applications. In the pursuit of a method to destabilize Mg_2NiH_4, numerous studies have been conducted to modify Mg_2Ni. Yang et al. [23] conducted experimental research wherein Mg_2Ni was alloyed with various transition metals (Ti, Cr, Mn, Fe, Co, Ni, Cu, and Zn). Their findings revealed that Ti and Cu showed the most promise as replacements for Ni in Mg_2Ni. Gasiorowski's [24] investigation suggested that the partial substitution of Mg with Mn or Al in Mg_2Ni alloy results in an increase in discharge capacity [15]. Liang et al. [25] discovered that partially substituting manganese with titanium decreased the activation energy of desorption from 69 kJ/mol for nanocrystalline Mg_2Ni to 59 kJ/mol for $Mg_{1.9}Ti_{0.1}Ni$. Modeling calculations using density functional theory (DFT) indicated that the enthalpy of hydrogenation for Mg_2Ni could be reduced by doping with Cu, Fe, Al, Ag, Ti, and Zn. They discovered that Ti and Cu showed the most potential as substitutes for Ni in Mg_2Ni. Qian Li [26] synthesized $Mg_{2-x}Ag_xNi$ (x = 0.05, 0.1, 0.5) through hydriding combustion synthesis and concluded that incorporating a small amount of silver (Ag) into Mg_2Ni is reasonable. This addition enhances the kinetics of the $Mg_{2-x}Ag_xNi$ (x = 0.05, 0.1) hydrogen storage alloy. Recently, Kalisvaart [27] and Chao Fan [28] conducted experimental studies on the hydrogen sorption properties of binary and ternary Mg-based alloys, incorporating Al, Fe, and Ti as alloying elements. They observed that the ternary alloys exhibited superior performance compared to the binary alloys. This improvement is likely attributed to the multiphase structure of the ternary alloys, where a main Mg storage phase is combined with Ti–Al or Ti–Fe intermetallic. These intermetallic phases act as pathways for enhanced hydrogen diffusion and as surface catalysts, thereby facilitating more efficient hydrogen sorption.

Several theoretical studies employing first-principles calculations have been conducted to investigate doped or substituted complex hydrides. Van Setten [29] examined the impact of doping Mg_2NiH_4 with transition metals through first-principles density functional theory calculations. The results indicated that substituting one in every eight Ni atoms with Cu or Fe can potentially reduce the hydrogen desorption enthalpy by approximately 0.1 eV/H_2. Ding et al. [30] conducted research on the use of silicon additives as interstitial atoms in Mg_2Ni through first-principles calculations. They observed that the addition of silicon atoms promotes the dehydrogenation reaction. However, the impact of silicon doping in Mg_2Ni and its hydrides has received limited attention in existing studies.

This study employed first-principles calculations to investigate the crystal structure, electronic structure, and thermodynamic impacts of iron doping in Mg_2Ni and Mg_2NiH_4. This work revealed that the hydrogen desorption enthalpy could be decreased from 65.17 to 52.72 kJ/mol H_2 when substituting one in sixteen magnesium atoms with Fe, and from 57.58 kJ/mol H_2 when substituting one in eight nickel atoms with Fe. This suggests potential practical applications.

2. Calculation models

Our calculations are performed using CASTEP is a widely used software package for performing ab initio quantum mechanical calculations on the electronic structure of materials. Developed by the Theory of Condensed Matter group at the University of Cambridge [31,32].This software utilizes plane-wave basis sets for handling valence electrons and employs pseudopotentials to approximate the potential field generated by ionic cores. The calculations utilized the Perdew–Burke–Ernzerhof (PBE) generalized gradient approximation (GGA) for the exchange and correlation potential [33]. Spin-polarized calculations were applied to Ni and Fe transition metals. To replace the core electrons, Ultrasoft pseudopotentials [34,35] in reciprocal space were utilized. All the Due to computational constraints, geometry optimization calculations were conducted with a 380 eV energy cut-off.This level of precision is satisfactory for achieving effective convergence in both forces exerted and the total energy on the atoms [13] for iron-doped Mg_2Ni and their hydrides. The associated k-point sets for both the pure and Fe-doped Mg_2Ni unit cells are $6 \times 6 \times 2$ and the calculations on Fe doped and undoped Mg_2NiH_4 unit cell utilized a $2 \times 4 \times 4$ k-point sets. The convergence criteria were established as follows: 5.0×10^{-6} eV/atom for energy change, 5.0×10^{-4} Å for maximum displacement, 0.01 eV/Å for maximum force, 0.02 GPa for maximum stress. The activation energy for diffusion can be determined through the transition state function in CASTEP. The algorithm used by CASTEP for this purpose is the "Complete LST/QST" method. This technique merges the standard LST/QST algorithm with the conjugate gradient method, facilitating a swift and dependable identification of the correct transition state [36,37]. Hence, the current calculations are sufficiently accurate to depict the fundamental properties of the ground states of these compounds.

3. Results and discussion

3.1. Structure parameters

First of all, the structure Mg_2Ni and Mg_2NiH_4 were optimized to assess the precision of the computational models. Mg_2Ni has a hexagonal structure as shown in Fig. 1(a), with lattice parameter a = 5.216 Å, c = 13.20 Å and space group $P6_222$ (180) [38]. The Mg_2Ni unit cell is represented by the chemical formula $Mg_{12}Ni_6$, consisting of 12 magnesium atoms occupy 6i and 6f lattice sites and 6 nickel atoms occupy 3b and 3d lattices sites. The unit cell structure of Mg_2NiH_4, depicted in belongs to the C2/c (15) space group, housing 16 magnesium atoms, 8 nickel atoms, and 32 hydrogen atoms occupy [39]. Structural optimization yielded the parameters for Mg_2Ni and Mg_2NiH_4, as detailed in Table 1 and compared with experimental data. The comparison reveals a significant degree of agreement between the computed results and experimental observations, confirming the precision of the computational model utilized in this investigation. To examine the impact of doping iron in Mg_2Ni and Mg_2NiH_4 on their structures, we replace one magnesium or nickel atom with a corresponding iron atom. As depicted in Figs. 1 and 2, the unit cells of Mg_2Ni and Mg_2NiH_4, upon doping with iron through the substitution of magnesium, are denoted as $Mg_{11}FeNi_6$ and $Mg_{15}FeNi_8H_{32}$, respectively. Similarly, the structures $Mg_{12}FeNi_5$ and $Mg_{16}FeNi_7H_{32}$ are obtained by replacing one nickel atom with iron

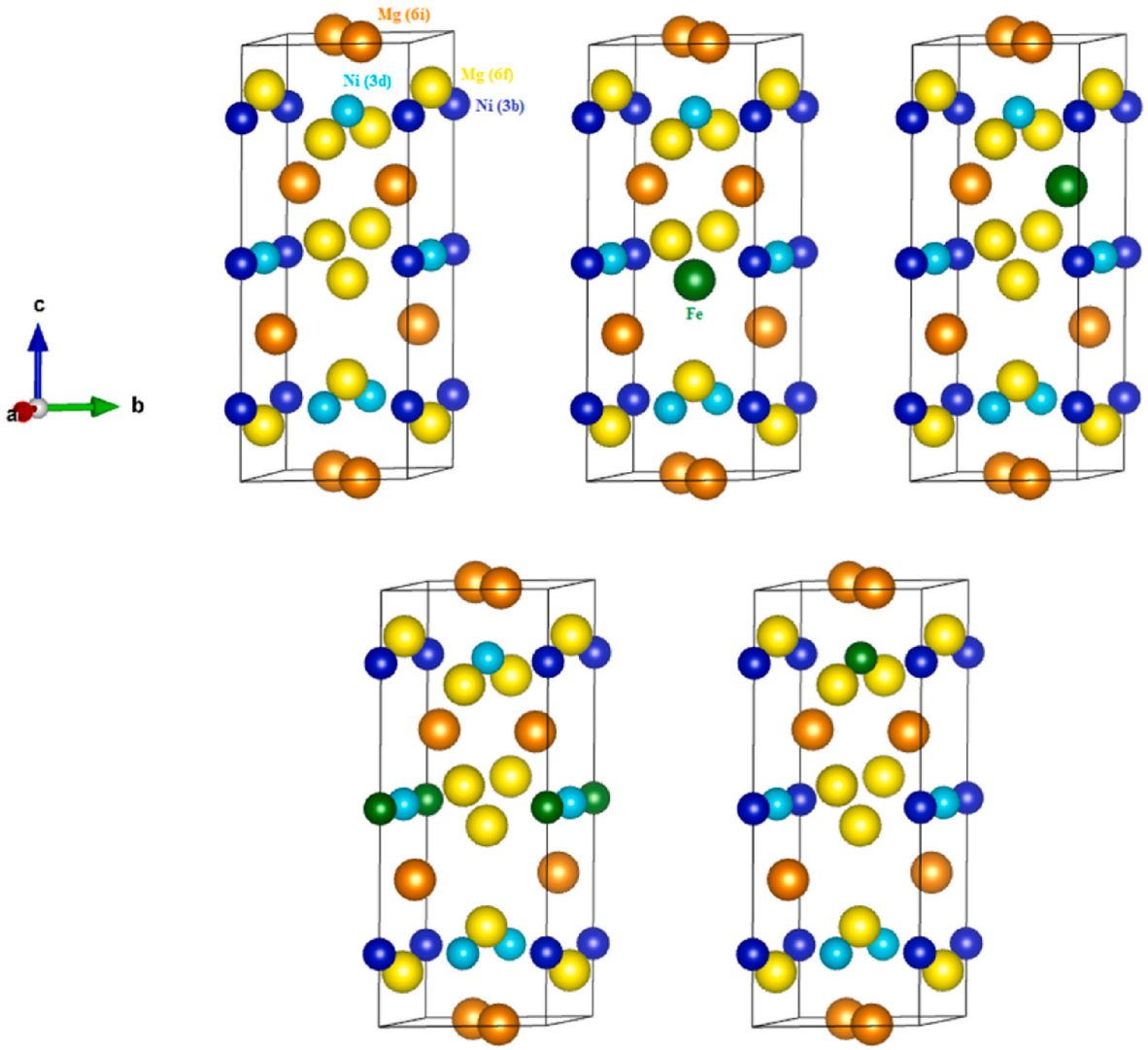

Fig. 1. Unit cell of Hexagonal Mg_2Ni (a), $Mg_{11}Fe_{Mg(6f)}\ Ni_6$ (b), $Mg_{11}Fe_{Mg(6i)}\ Ni_6$ (c), $Mg_{12}Fe_{Ni(3b)}\ Ni_5$ (d), $Mg_{12}Fe_{Ni(3d)}\ Ni_5$ (e) (Where Orange, Yellow, Blue, light blue and green balls denote Mg(6f), Mg(6i), Ni(3b), Ni(3d) and Fe positions respectively).

Table 1
Calculated and Experimental structural parameters of Mg_2Ni and Mg_2NiH_4 phase.

Compound	Lattice constants of unit cell (Å)		Atomic Positions	Fractional coordinates of atoms					
	calculated	experimental		calculated			experimental		
Mg_2Ni ($P6_222$)	a = 5.217(8)	a = 5.216 [38]	Mg_1 (6f)	1/2	0	0.165(6)	1/2	0	0.1149 [61]
	c = 13.24(6)	c = 13.20	Mg_2 (6i)	0.165(2)	0.330(5)	0	0.163	0.327	0
	γ = 120°	γ = 120°	Ni_1 (3b)	0	0	1/2	0	0	1/2
			Ni_2 (3d)	1/2	0	1/2	1/2	0	1/2
Mg_2NiH_4 (C_2/c)	a = 14.223	a = 14.343 [39,62]	Mg_1 (4e)	0	0.0221	3/4	0	0.0144	3/4 [38]
	b = 6.343	b = 6.4038	Mg_2 (4e)	0	0.5284	3/4	0	0.5130	3/4
	c = 6.419	c = 6.4830	Mg_3 (8f)	0.2458	0.4852	0.0799	0.2652	0.4827	0.0754
	β = 113.33(3)°	β = 113.52°	Ni (8f)	0.1188	0.2315	0.0836	0.1194	0.2308	0.0832
			H_1 (8f)	0.205	0.3096	0.3036	0.2113	0.2995	0.3037
			H_2 (8f)	0.1379	0.3184	0.8759	0.1360	0.3163	0.8811
			H_3 (8f)	0.0096	0.2897	0.0255	0.0105	0.2868	0.0537
			H_4 (8f)	0.1296	0.9885	0.0741	0.1306	0.995	0.0815

in the unit cells of Mg_2Ni and Mg_2NiH_4, respectively. Table 2 presents the structural parameters of $Mg_{12}Ni_6$ unit cells with single iron (Fe) atom doping. It can be seen that the impact of enlarging the original lattice, caused by substituting iron (Fe) for nickel (Ni), is more pronounced compared to substituting Fe for magnesium (Mg). The metallic atomic radius of Mg, Fe and Ni are 1.6, 1.26 and 1.24 respectively. The electronegativity of Fe (1.83) surpasses that of Mg (1.31) but fall short that Ni (1.91) implying a stronger interaction between Ni and Fe atoms compared to Mg and Fe atoms. This is because the atomic radii of Fe are smaller than Mg but larger than Ni, resulting in higher electronegativities for Fe compared to Mg but lower than Ni. Consequently, the crystal constants of Mg_2Ni expand or contract to varying degrees when

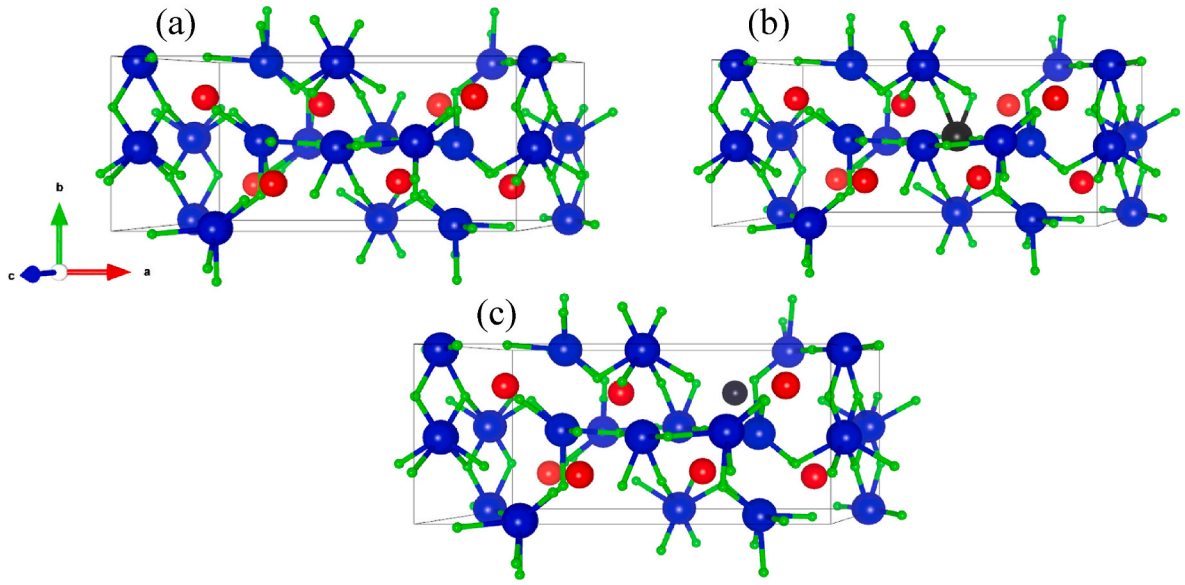

Fig. 2. Unit cell of Monoclinic Mg_2NiH_4 (a), $Mg_{15}FeNi_8H_{32}$ (b), $Mg_{16}FeNi_7H_{32}$ (c).

Table 2
Structural parameters of Fe-doped Mg_2Ni.

Cell parameter	a (Å)	b (Å)	c (Å)	V(Å^3)	γ (°)
$\mathbf{Mg_{11}Fe_{Mg(6f)}\,Ni_6}$	5.095	5.138	13.109	298.126	119.693
$\mathbf{Mg_{11}Fe_{Mg(6i)}\,Ni_6}$	5.118	5.190	12.987	297.926	119.739
$\mathbf{Mg_{12}Fe_{Ni(3b)}\,Ni_5}$	5.152	5.224	13.323	312.201	119.489
$\mathbf{Mg_{12}Fe_{Ni(3d)}\,Ni_5}$	5.228	5.228	13.291	311.625	120.936

substituted with Fe due to the aforementioned factors. The substitution of both Mg and Ni with Fe in Mg_2NiH_4 without any change in lattice parameters can be explained by forming a solid solution with both Mg and Ni, allowing it to substitute for these atoms without causing major changes in the crystal structure.

3.2. Enthalpy of formation and decomposition temperature of Fe-doped Mg_2Ni and their hydrides

The enthalpy of formation of a compound is established by subtracting the energies of its constituent elements in their stable configurations from its total energy. This measurement serves as an indication of the thermodynamic preference and degree to which the compound structure is favored compared to its individual elements. Thus, for a lattice composed of x magnesium (Mg) atoms, y iron (Fe) atoms, and z nickel (Ni) atoms, the enthalpy of formation is expressed as follows:

$$\Delta_f H\left(Mg_xFe_yNi_z\right) = E_{tot}\left(Mg_xFe_yNi_z\right) - [x\,E(Mg) + y\,E(Fe) + z\,E(Ni)] \quad (1)$$

In this context, E_{tot} and $\Delta_f H$ stand for the total energy and formation enthalpy of the compound. Meanwhile, E(Mg), E(Fe), and E(Ni) refer to the specific atomic energies of hcp-Mg, α-Fe, and fcc-Ni in their solid states, respectively. Similarly, hydrogenation reaction for iron doped $Mg_{11}FeNi_6$ and $Mg_{12}Ni_5Fe$ are:

$$\frac{1}{12}\,M_{12}N_6 + H_2 = \frac{1}{16}Mg_{16}Ni_8H_{32} \quad (2)$$

Referred to the equation [40]:

$$Mg_2Ni + 2H_2 = Mg_2NiH_4 \quad (3)$$

Thus, the enthalpy of hydrogenation can be computed using the formula:

$$\Delta_f H\left(Mg_{16}Ni_8H_{32}\right) = \frac{1}{16}E_{tot}\left(Mg_{16}Ni_8H_{32}\right) - \left[\frac{1}{12}E(Mg_{12}Ni_6) + E(H_2)\right] \quad (4)$$

In this case, the corresponding formation reaction for hydride substitution $Mg_{11}FeNi_6$ and $Mg_{12}FeNi_5$ with iron (Fe) is:

$$\frac{1}{12}Mg_{11}FeNi_6 + \frac{1}{12}Mg + \frac{11}{12}Fe + H_2 = \frac{1}{16}Mg_{15}FeNi_8H_{32} + \frac{1}{16}Mg + \frac{15}{16}Fe \quad (5.a)$$

$$\frac{1}{12}Mg_{12}FeNi_5 + \frac{1}{12}Ni + \frac{11}{12}Fe + H_2 = \frac{1}{16}Mg_{16}FeNi_7H_{32} + \frac{1}{16}Ni + \frac{15}{16}Fe \quad (5.b)$$

And the variation of enthalpy of the reactions involving Fe substitution in $Mg_{15}FeNi_8H_{32}$ and $Mg_{16}FeNi_7H_{32}$ can be determined using the following equation:

$$\Delta_f H\left(Mg_{15}FeNi_8H_{32}\right) = \frac{1}{16}E_{tot}\left(Mg_{15}FeNi_8H_{32}\right) - \frac{1}{12}E(Mg_{11}FeNi_6) - E(H_2) - \frac{1}{48}E(Mg) + \frac{1}{48}E(Fe) \quad (6)$$

$$\Delta_f H\left(Mg_{16}FeNi_7H_{32}\right) = \frac{1}{16}E_{tot}\left(Mg_{16}FeNi_7H_{32}\right) - \frac{1}{12}E(Mg_{12}FeNi_5) - E(H_2) - \frac{1}{48}E(Ni) + \frac{1}{48}E(Fe) \quad (7)$$

The total energies of compounds, such as $Mg_{12}Ni_6$, $Mg_{16}Ni_8H_{32}$, $Mg_{11}Fe_{Mg(6f)}Ni_6$, $Mg_{11}Fe_{Mg(6i)}Ni_6$, $Mg_{12}FeNi_{(3b)}Ni_5$, $Mg_{12}FeNi_{(3b)}Ni_5$, $Mg_{15}FeNi_8H_{32}$, $Mg_{16}FeNi_7H_{32}$, as well as individual elements Mg, Ni, Fe, and H_2, were computed and are presented in Table 3 and illustrated in Fig. 3. It is apparent that the formation enthalpy of Mg_2Ni is −3.5792 eV. This enthalpy of formation has the most negative value indicating that it is more stable and become instable when doping Fe in Ni(3d), Ni (3b), Mg(6i) and Mg(6f) positions with $\Delta_f H$ were −2.2607 eV, −2.1801 eV, −2.1475 eV, and −1.9527 eV respectively. The current computation of enthalpy of formation indicates that pure Mg_2Ni phase exhibit greater thermodynamic favorability compared to the Fe-doped phases. Consequently, the calculated enthalpy of formation affirms that the most favorable location for the substitution of Fe within the Mg_2Ni lattice is at the Ni(3d) position. Similarly, with regards to doped Mg_2NiH_4, with an enthalpy of formation equal to −0,6754 eV. This can be translated to

Table 3
Calculated Total energy and enthalpy of formation.

Compound	Total energy (eV)	Enthalpy of formation of unit cell		Temperature of Decomposition (K)
		[eV]	[kJ/mol. H_2]	
Mg	−973.9476			
Fe	−864.916			
Ni	−1354.3881			
H_2	−31.5652			
$Mg_{12}Ni_6$	−19817.2794	−3.5792	−345.366	
$Mg_{11}Fe_{Mg\ (6f)}Ni_6$	−19706.6273	−1.9587	−189.002	
$Mg_{11}Fe_{Mg\ (6i)}Ni_6$	−19706.8161	−2.1475	−207.219	
$Mg_{12}Fe_{Ni\ (3b)}Ni_5$	−19326.4081	−2.1801	−210.361	
$Mg_{12}Fe_{Ni\ (3d)}Ni_5$	−19326.4887	−2.2607	−218.138	
$Mg_{16}Ni_8H_{32}$	−26938.8900	−0.6754	−65.1704	501.3108
$Mg_{15}Fe_{Mg\ (6i)}Ni_8H_{32}$	−26828.5533	−0.5257	−50.7266	390.1969
$Mg_{15}Fe_{Mg\ (6f)}Ni_8H_{32}$	−26828.5412	−0.5415	−52.2454	401.8876
$Mg_{16}Fe_{Ni\ (3b)}Ni_7H_{32}$	−26449.4330	−0.6036	−58.2404	448.0030
$Mg_{16}Fe_{Ni\ (3d)}Ni_7H_{32}$	−26446.4020	−0.5969	−57.5920	442.9708

−65.1704 kJ/mol H_2, which is in a good agreement with experimental calculation of −64.3 kJ/mol referred in Ref. [41]. A notable discovery is that Fe doping leads to a significant reduction in the reaction enthalpy with doping Mg, reaching −50.72 kJ/mol H_2 for $Mg_{15}FeNi_8H_{32}$ and the reaction enthalpy with doping Ni, reaching −57.58 kJ/mol H_2 for $Mg_{16}FeNi_7H_{32}$. In contrast to the doping of transition metal elements as previously reported, such as −51.56 kJ/mol H_2 for Al, −53.63 kJ/mol H_2 for Ag [40], −51.93 kJ/mol H_2 for $Mg_2Ni_{0.875}Zn_{0.125}H_4$ [42] and −46.2 kJ/mol H_2 for $Mg_{16}Ni_7SiH_{32}$ [43]. This can be explained by the destability of the alloys and the $Mg_{15}FeNi_8H_{32}$ hydride. To summarize, we can conclude that substituting some Mg with Fe in a specific site positively affects the dehydrogenation properties of Mg_2NiH_4 hydride, which strongly supports earlier experimental observations [44] and theoretical predictions [29,40].

The second crucial parameter determined after the formation enthalpy is the decomposition temperature (T_d), which is vital for choosing suitable hydrogen storage materials [18,45,46]. The decomposition temperature was calculated using Van't Hoff's law (Equation (8)) as follows:

$$\Delta G = \Delta H - T\Delta S \tag{8}$$

At equilibrium, the standard Gibbs energy is assumed to be negligible, and the entropy primarily arises from the release of hydrogen gas, with a value of $\Delta S(H_2) = 130$ J/mol.K.

Therefore, the following equation will be employed to calculate the decomposition temperature [47,48] (equation (9)):

$$T_{d=}\frac{\Delta H}{130} \tag{9}$$

The decomposition temperature of undoped Mg_2NiH_4 is therefore 501.3108 K which aligns well with the recent studies indicate that Mg_2NiH_4 undergoes dehydrogenation at temperatures around 503–578 K [49–51], but this value still exceeds the operational temperature range for PEM fuel cells, which spans from 289 K to 393 K [52].

To enhance the temperature of decomposition, we substituted Fe with Mg and Ni as we did with the formation enthalpy. Fig. 3 and Table 3 summarized the variation of T_d in different site of substitution. We can conclude that substituting Fe with Mg specifically in the 6i site greatly reduces the decomposition temperature and significantly affects stability as the decomposition temperature approaches the operating temperature of PEM fuel cells closely.

3.3. Density of state (DOS)

In order to elucidate the bonding interactions in Fe doping alloys and hydrides and comprehend their stability and dehydrogenation characteristics, we calculate and compare the total (DOS) and partial density of states (PDOS) per atom for both undoped and doped compounds, as depicted in Figs. 4 and 5. The computed total density of states (TDOS) for Mg_2Ni and Mg_2NiH_4 closely aligns with findings from prior studies [43,53–55,63]. In these figures, the Fermi level (E_F) is designated as zero and serves as a point of reference. Fig. 4a represent the Total and partial density of state of pure Mg_2Ni with no band gap that indicate a metallic behavior. It illustrates that the primary bonding peaks fall within the

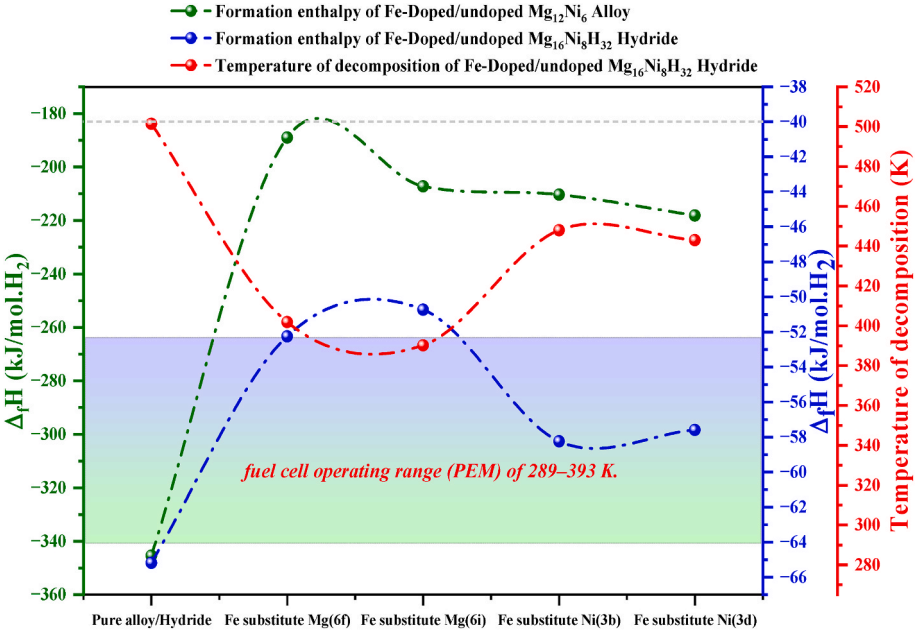

Fig. 3. The formation enthalpies and Temperature of decomposition of Fe-Doped and undoped alloys and hydrides.

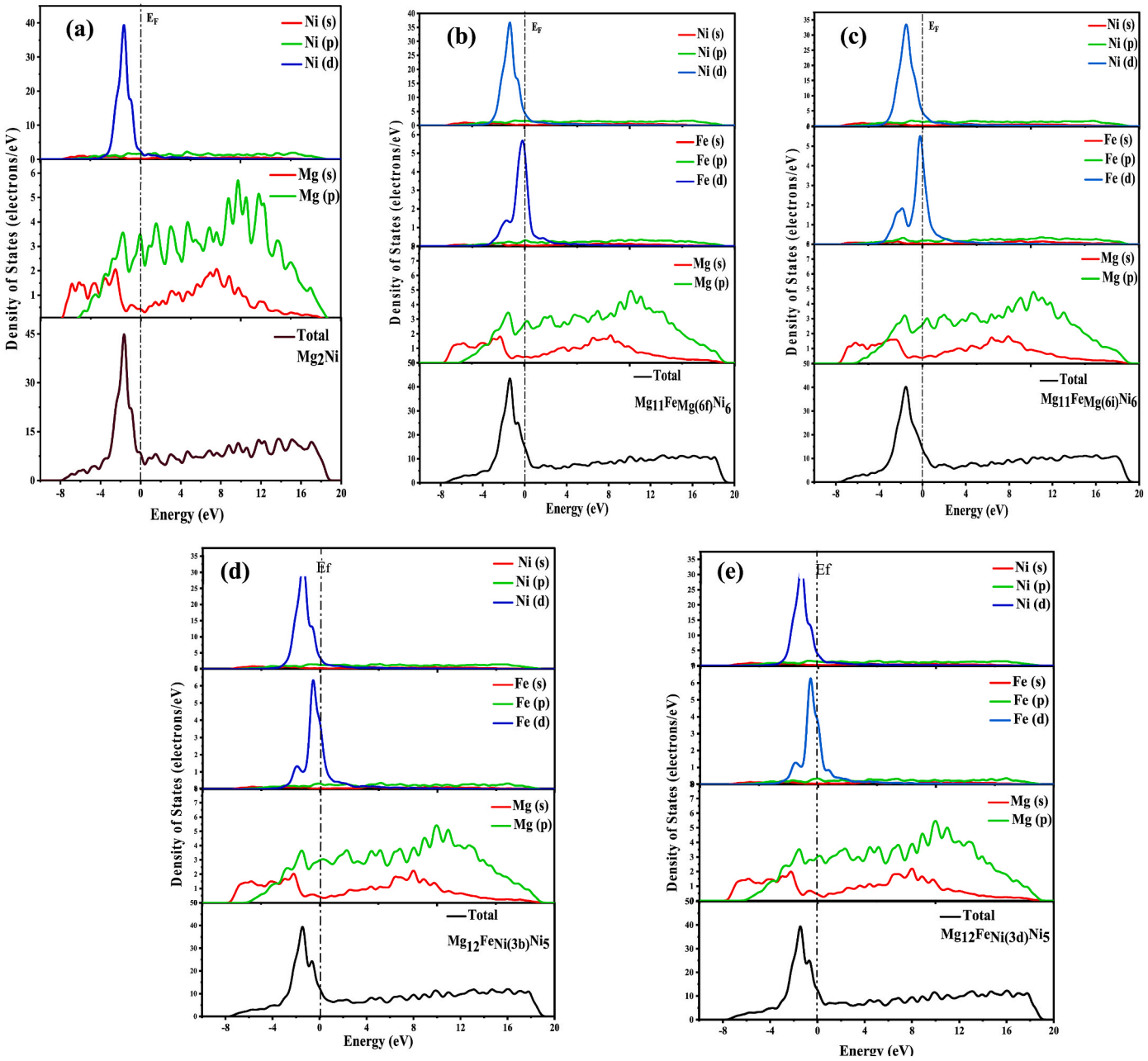

Fig. 4. Total DOS and corresponding partial DOS for Mg_2Ni (a), $Mg_{11}Fe_{Mg(6f)}Ni_6$ (b), $Mg_{11}Fe_{Mg(6i)}Ni_6$ (c), $Mg_{12}Fe_{Ni(3b)}Ni_5$ (d), $Mg_{12}Fe_{Ni(3d)}Ni_5$ (e).

energy range of −7.68eV to the Fermi level (E_F). At −1.66 eV, the highest peak, primarily arises from the Ni d electrons, accompanied by contributions from the Mg s, Mg p, and a small fraction of Ni p electrons. The bonding peaks spanning from −6.32 eV to −3.47 eV originate from the combined effects of Mg (s), Mg(p), Ni(s), and Ni(p) orbitals. Additionally, the bonding peaks from −7.6 eV to −6.32 eV are predominantly governed by Mg(s) electrons, with a minor contribution from Ni (s) electrons. These findings suggest extensive hybridization between Mg and Ni atomic orbitals, with the strong bonding interactions between Mg(s), Mg(p), and Ni(d) electrons playing a dominant role in controlling the structural stability of the Mg_2Ni phase. The density of states (DOS) for $Mg_{11}Fe_{Mg(6f)}Ni_6$ and $Mg_{11}Fe_{Mg(6i)}Ni_6$ exhibits a close resemblance, mirroring the minimal difference in their calculated enthalpies of formation, as discussed earlier. Similarly, the DOS for $Mg_{12}Fe_{Ni(3b)}Ni_5$ and $Mg_{12}Fe_{Ni(3b)}Ni_5$ also demonstrates a comparable pattern. For Fe-doped Mg_2Ni unit cells, differences in the density of states (DOS) depicted in Fig. 4b, c, d, e, and f are noticeable.

(1) In comparison to the pure Mg_2Ni unit cell, the height of bonding peaks involving Mg(s), Mg(p), and Ni(d) decreases between −4.0 eV and the Fermi level (E_F) for $Mg_{11}Fe_{Mg(6f)}Ni_6$, $Mg_{11}Fe_{Mg(6i)}Ni_6$, $Mg_{12}Fe_{Ni(3b)}Ni_5$, and $Mg_{12}Fe_{Ni(3d)}Ni_5$.

(2) As a result of Fe substitution, the Fe s, Fe p, and Fe d orbitals engage in bonding with Ni and Mg atomic orbitals within the energy range of −4.0 to E_F (0 eV). The first observation suggests a weakening of the interaction among Mg s, Mg p, and Ni d orbitals, leading to the destabilization of the unit cells. The primary interaction between Mg and Ni atoms remains the most significant, as it upholds the structural integrity of the unit cell. Therefore, despite the bonding among Mg, Ni, and Fe atoms, the reduction in Mg–Ni atomic interaction diminishes the stability of Fe-doped phases, aligning with the calculated enthalpy of formation results. Fig. 5a shows the density of state of undoped Mg_2NiH_4 which exhibits two distinct energy gaps: a fundamental gap and a valence gap, situated between the Fermi level (E_F) and

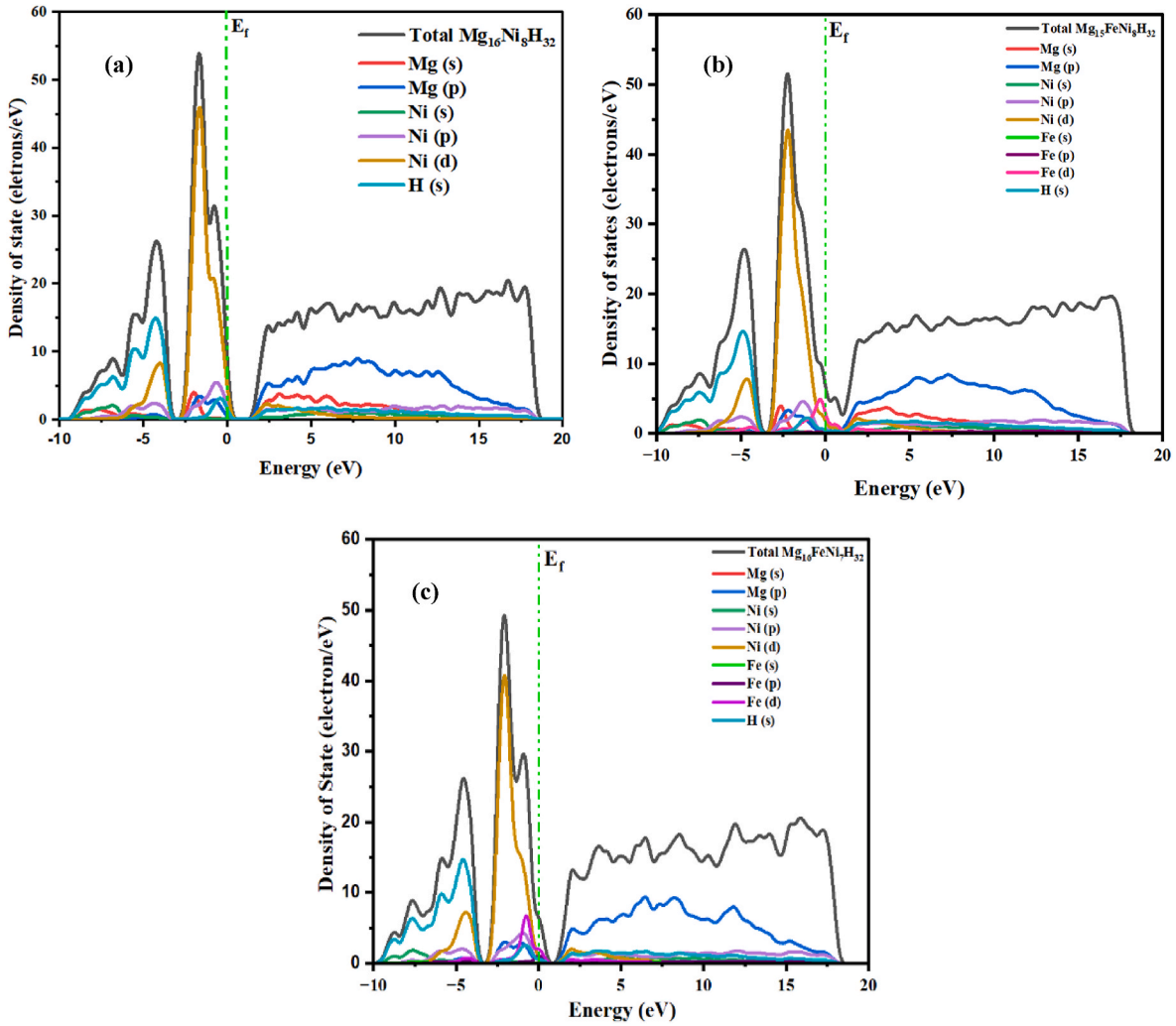

Fig. 5. Total and partial density of states of $Mg_{16}Ni_8H_{32}$ (a), $Mg_{15}FeNi_8H_{32}$ (b) and $Mg_{16}FeNi_7H_{32}$ (c).

1.34eV, −2.66eV, and −3.34ev, respectively. The bonding peaks spanning from the Fermi level (E_F) to −2.66 eV primarily stem from the contributions of valence electrons from Ni(3d), H(s), and a small fraction of Mg(3s) (2p) orbitals. Between −3.34 and −6 eV, the bonding peaks result from interactions between H(s) and Ni(3d), as well as a few Mg(3s) (2p) electrons. Furthermore, the bonding peaks observed between −6 and −9 eV are mainly governed by the valence electrons of H(s), Ni(4s), and a few Mg (3s) orbitals. Clearly, there exists a significant hybridization between Ni(3d) (4s) and H(s) orbitals compared to that between Mg (3s) (2p) and H(s) orbitals, indicating that the Ni–H bonding interaction is stronger than that of Mg–H in Mg_2NiH_4 hydride. The outcomes align with other computational investigations [54]. Following Fe doping, as depicted in Fig. 5(b) and (c), the density of states (DOS) and partial density of states (pDOS) plots shift towards lower energy levels compared to the undoped case. When Fe is introduced as a dopant in Mg, it decreased the direct gap significantly and adds extra states within both the fundamental and valence energy gaps. This phenomenon leads to the reduction or elimination of these energy gaps. In other words, the introduction of Fe in Mg disrupts the existing energy band structure of the material, causing the energy gaps to narrow or vanish altogether. This effect is significant as it alters the electronic properties of the material, potentially influencing its behavior and performance in various applications. Hence, the destabilization of Mg_2NiH_4 due to Fe doping can be attributed to several factors. Firstly, the interactions between Mg and Ni (Mg–Ni) and between Ni and H (Ni–H) are weakened by the introduction of Fe. Secondly, there is a decrease in the number of bonding electrons below the Fermi level (E_F) as a result of Fe doping. Hence, the introduction of doping may decrease the stability of the hydride system. This outcome aligns with the calculated enthalpies of formation. These factors are intrinsic to the system and contribute to the enhancement of the dehydrogenation properties of Mg_2NiH_4 hydride.

3.4. Ionic conductivity

The ionic conductivity of metal hydrides is crucial for hydrogen storage, as it impacts the efficiency of hydrogen absorption and desorption. Enhanced ionic conductivity improves hydrogen diffusion and kinetics, which is vital for applications requiring rapid cycling and high efficiency, such us PEM fuel cells. Research focuses on optimizing material properties to enhance storage capacity and performance, with factors such as temperature, pressure, and alloying elements significantly influencing ionic conductivity and overall system efficiency. Understanding these factors is essential for developing advanced hydrogen storage materials for modern energy applications [56–59].

The ionic conductivity (σ) of pure and doped Mg_2NiH_4 hydride can be calculated using the following equation:

$$\sigma = \frac{2}{3}\left[\frac{(Ze)^2}{kTm} n E_a \tau_0 \exp\left[\frac{-E_a}{kT}\right]\right] \quad (10)$$

$$\tau_0 = \frac{I}{v} \quad (11)$$

$$v = \sqrt{\frac{2 \times E_a}{m}} \quad (12)$$

Where the constants are tabulated in Nomenclature table and I is equal to 2.46 Å,. The diffusion activation energies are shown in Fig. 6. As illustrated, the activation energy decreases from 0.53 eV for $Mg_{12}Ni_8H_{32}$ to 0.49 eV for $Mg_{12}FeNi_7H_{32}$ and further to 0.44 eV for $Mg_{15}FeNiH_{32}$. This reduction in activation energy is attributed to the variation in distance between neighboring sites. The ionic conductivity calculated using equation (10) and illustrated in Fig. 7 shows that σ is also influenced by the substitution of Mg and Ni with Fe. In our system, the ionic conductivity of pure Mg_2NiH_4 is 3.84×10^{-4} S/cm at room temperature (300K), which agrees with experimental results [60].

The comparison of ln(σ) versus 10^3/T in Fig. 8 demonstrates a strong agreement between theoretical and experimental data. The similar slopes confirm that the activation energies for ionic conductivity are effectively captured by the theoretical model, affirming its reliability. This concordance reinforces the validity of the theoretical approach and supports its use in analyzing and predicting ionic conductivity in hydrogen storage materials. In contrast, the ionic conductivity of $Mg_{16}FeNi_7H_{32}$ and $Mg_{15}FeNi_8H_{32}$ is 8.16×10^{-4} S/cm and 1.1910^{-3} S/cm, at room temperature respectively. This demonstrates that the ionic conductivity increases with the destabilization of the material, reaching up to 1.12×10^{-1} S/cm for $Mg_{15}FeNi_8H_{32}$ at 400K. The slight deviation in absolute conductivity values particularly the offset observed in the vertical scale is attributed primarily to intrinsic limitations in the idealized assumptions of the model, such as perfect crystallinity, absence of grain boundaries, and neglect of defect-related scattering mechanisms, all of which can impact carrier mobility in real samples. Additionally, environmental variables such as pressure, microstructure, and sample purity in experimental setups may further contribute to the observed offset.

When iron (Fe) substitutes magnesium (Mg) in the Mg_2NiH_4 lattice, the introduced 3d electrons from Fe contribute significantly to the conduction band, modifying the electronic structure. Magnesium, an alkaline earth metal, primarily supplies s-electrons that lie far below the Fermi level and play a limited role in electrical conduction. In contrast, Fe introduces localized 3d states near the Fermi level, thereby increasing the density of states (DOS) in this region. This enhanced DOS facilitates greater charge carrier availability and improved electronic interactions, ultimately contributing to higher ionic conductivity. Furthermore, the Fe 3d orbitals exhibit stronger hybridization with neighboring s and p orbitals, promoting better charge transport and lowering the activation energy required for ionic migration.

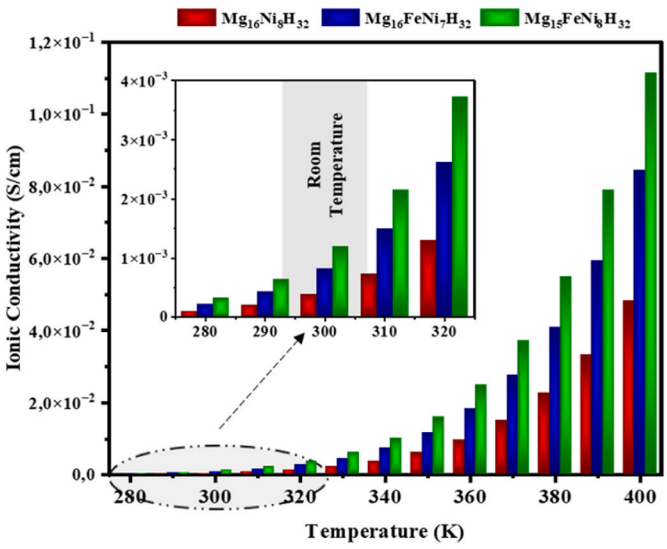

Fig. 7. Evolution of ionic conductivity as a function of temperature.

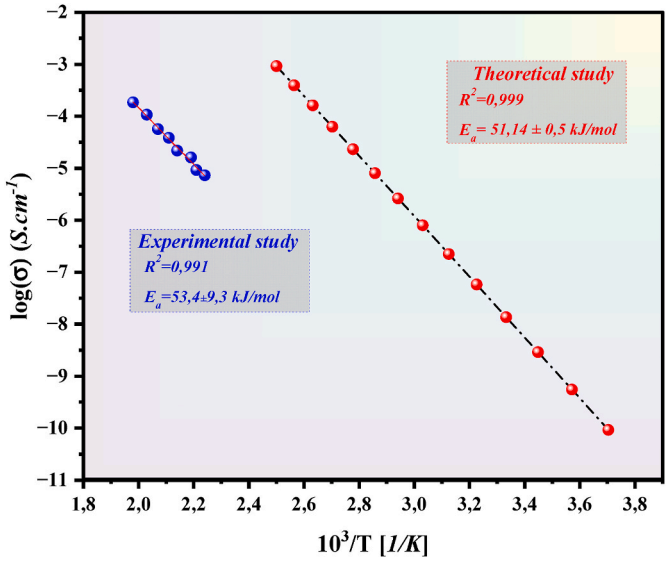

Fig. 8. Comparison of the theoretical and experimental studies of the logarithm of ionic conductivity log(σ)) plotted against the reciprocal temperature (10^3/T).

In comparison, when Fe replaces nickel (Ni), the effect on conductivity is less pronounced. Both Fe and Ni are transition metals with similar 3d electron configurations, and Ni already contributes d-

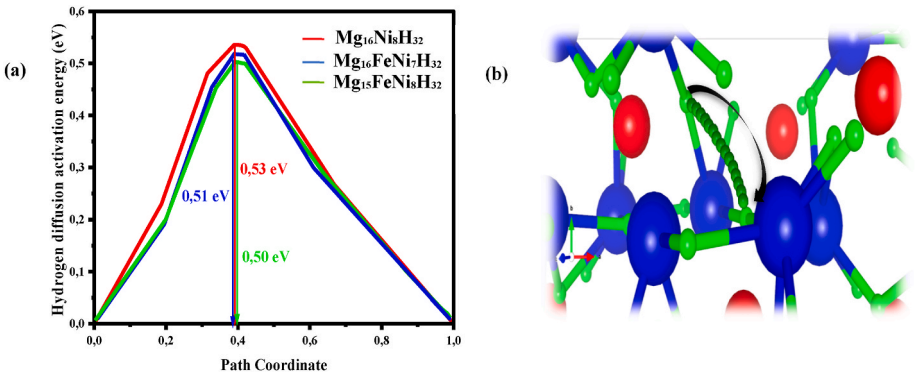

Fig. 6. H diffusion activation energy diagram (a). H adsorption sites and migration pathways (b).

electrons close to the Fermi level. Consequently, Fe-for-Ni substitution results in minimal modifications to the DOS and conduction band, leading to only a modest improvement in ionic conductivity.

Overall, changes in the electronic density and orbital hybridization introduced by Fe, particularly when substituting Mg facilitate more efficient ionic transport by reducing the migration barrier. These effects underscore the potential of Fe-doped Mg_2NiH_4 as a promising candidate for advanced hydrogen storage applications, where enhanced ionic conductivity is critical for high-performance operation.

4. Conclusions

Utilizing the first-principles calculations method grounded in density functional theory (DFT) with CASTEP software, an in-depth investigation into the dehydrogenation properties and underlying micro mechanism of Fe-doped Mg_2Ni and their hydride Mg_2NiH_4 is systematically conducted. The principal conclusions are outlined as follow:

1 The computed lattice parameters and atomic coordinates closely match experimental findings. The enthalpy of formation calculations indicate that the pure Mg_2Ni phase is thermodynamically more favorable than the Fe-doped phases. Furthermore, the potential sites for Fe substitution within the Mg_2Ni lattice have been identified, with confirmed preferences in the following order: Mg(6f) < Mg(6i) < Ni(3b) < Ni(3d) positions.
2 The substitution of Fe diminishes the stability of Mg_2NiH_4, as evidenced by the decrease information enthalpy. However, in comparison, the enhancement in dehydrogenation performance due to doping Fe with Mg substitution is superior to that of Ni.
3 Analysis of the density of states (DOS) suggests that the predominant factor governing the structural stability of both pure and Fe-doped Mg_2Ni phases is the strong hybridization between Mg s, Mg p, and Ni d electrons. However, the substitution of Fe for Mg and Ni atoms in the Mg_2Ni unit cell weakens the interaction between Mg s, Mg p, and Ni d electrons. However, the destabilization of Fe doped Mg_2NiH_4 is more favorable when doping Mg than Ni. The findings from the analysis of the density of states (DOS) align with those obtained from the calculation of enthalpies of formation.
4 The ionic conductivity of Mg_2NiH_4 increases significantly with Fe substitution, rising from 4.81×10^{-2} S/cm to 1.12×10^{-1} S/cm at 400 K. Fe substitution for Mg introduces additional d-electrons, enhancing charge carrier mobility, while Fe doping in Ni has a smaller effect due to similar electronic configurations. Theoretical and experimental results show good agreement in terms of temperature-dependent conductivity.

CRediT authorship contribution statement

Ikram Belkoufa: Writing – original draft, Software, Formal analysis, Data curation, Conceptualization. **Abdelmajid Assila:** Data curation, Conceptualization. **Seddiq Sebbahi:** Formal analysis, Data curation. **Amine Alaoui-Belghiti:** Validation, Supervision, Methodology, Investigation. **Said Laasri:** Visualization, Supervision. **Mouhaydine Tlemçani:** Visualization, Validation. **El Kebir Hlil:** Visualization, Validation, Supervision, Software, Methodology. **Abdelowahed Hajjaji:** Supervision, Project administration.

Declaration of competing interest

The authors declare that they have no known competing financial interests or personal relationships that could have appeared to influence the work reported in this paper.

Data availability

The data that has been used is confidential.

References

[1] J.O. Abe, A.P.I. Popoola, E. Ajenifuja, O.M. Popoola, Hydrogen energy, economy and storage: review and recommendation, Int. J. Hydrogen Energy 44 (2019) 15072–15086, https://doi.org/10.1016/j.ijhydene.2019.04.068.
[2] N.A.A. Rusman, M. Dahari, A review on the current progress of metal hydrides material for solid-state hydrogen storage applications, Int. J. Hydrogen Energy 41 (2016) 12108–12126, https://doi.org/10.1016/j.ijhydene.2016.05.244.
[3] B. Bogdanović, M. Felderhoff, S. Kaskel, A. Pommerin, K. Schlichte, F. Schüth, Improved hydrogen storage properties of Ti-doped sodium alanate using titanium nanoparticles as doping agents, Adv. Mater. 15 (2003) 1012–1015, https://doi.org/10.1002/adma.200304711.
[4] A. Assila, M. Rkhis, S. Sebbahi, A. Alaoui Belghiti, S. Laasri, E.K. Hlil, et al., Improvement of the thermodynamic properties of lithium borohydride $LiBH_4$ by mechanical treatment for hydrogen storage applications: a DFT investigation, Int. J. Hydrogen Energy 51 (2024) 72–78, https://doi.org/10.1016/j.ijhydene.2023.10.317.
[5] V.A. Yartys, M.V. Lototskyy, E. Akiba, R. Albert, V.E. Antonov, J.R. Ares, et al., Magnesium based materials for hydrogen based energy storage: past, present and future, Int. J. Hydrogen Energy 44 (2019) 7809–7859, https://doi.org/10.1016/j.ijhydene.2018.12.212.
[6] A. Razouk, M. El Kassaoui, M. Boubkri, A. Benyoussef, O. Mounkachi, Enhanced hydrogenation properties of two-dimensional MgH_2 by doping, vacancy-like defects and strain engineering: a theoretical study, Int. J. Hydrogen Energy 92 (2024) 1078–1090, https://doi.org/10.1016/j.ijhydene.2024.10.357.
[7] V.A. Yartys, M.V. Lototskyy, Laves type intermetallic compounds as hydrogen storage materials: a review, J. Alloys Compd. 916 (2022) 165219, https://doi.org/10.1016/j.jallcom.2022.165219.
[8] N. Hariti, A. Assila, M. Rkhis, S. Laasri, F. Belhora, M.E. Idrissi, et al., Density functional theory calculations applied to olivine-like $NaMnPO_4$ with transition metal substitutions for energy storage applications, Eur. Phys. J. Appl. Phys. 99 (2024) 20, https://doi.org/10.1051/epjap/2024240037.
[9] A. Alaoui-Belghiti, A. Assila, I. Belkoufa, M. Rkhis, S. Laasri, M. Tlemçani, et al., Strain engineering for optimized hydrogen storage: enhancing ionic conductivity and achieving near-room-temperature desorption in Mg_2NiH_4, Int. J. Hydrogen Energy 92 (2024) 1069–1077, https://doi.org/10.1016/j.ijhydene.2024.10.292.
[10] A.R. Paul, S. Mehla, S. Bhargava, Intermetallic compounds for hydrogen storage: current status and future perspectives, Small 21 (2025) 2408889, https://doi.org/10.1002/smll.202408889.
[11] L. Schlapbach, A. Züttel, Hydrogen-storage materials for mobile applications, Nature 414 (2001) 353–358, https://doi.org/10.1038/35104634.
[12] I.P. Jain, C. Lal, A. Jain, Hydrogen storage in Mg: a most promising material, Int. J. Hydrogen Energy 35 (2010) 5133–5144, https://doi.org/10.1016/j.ijhydene.2009.08.088.
[13] Optimizing hydrogen storage properties in Mg-based materials with multicomponent and high-entropy catalysts n.d. http://ijmmm.ustb.edu.cn/article/doi/10.1007/s12613-025-3149-z (accessed May 15, 2025).
[14] T. Liu, C. Wang, Y. Wu, Mg-based nanocomposites with improved hydrogen storage performances, Int. J. Hydrogen Energy 39 (2014) 14262–14274, https://doi.org/10.1016/j.ijhydene.2014.03.125.
[15] C. Shang, Z. Guo, Structural and desorption characterisations of milled (MgH_2+Y, Ce)(MgH_2+Y,Ce) powder mixtures for hydrogen storage, Int. J. Hydrogen Energy 32 (2007) 2920–2925, https://doi.org/10.1016/j.ijhydene.2006.11.035.
[16] H. Shao, K. Asano, H. Enoki, E. Akiba, Preparation and hydrogen storage properties of nanostructured Mg–Ni BCC alloys, J. Alloys Compd. 477 (2009) 301–306, https://doi.org/10.1016/j.jallcom.2008.11.004.
[17] H. Kim, et al., Insight into the hydrogenation properties of mechanically alloyed Mg50Co50 from the local structure, J. Phys. Chem. C n.d. 115 (2011) 20335–20341, https://doi.org/10.1021/jp207197k.
[18] I. Belkoufa, B. Misski, A. Alaoui-Belghiti, C. Moslah, M. Mouyane, D. Houivet, et al., Improved thermodynamic properties of (Sc, V, Ti, Fe, Mn, Co, and Ni) doped $NaBH_4$ for hydrogen storage: first-principal calculation, Int. J. Hydrogen Energy 68 (2024) 481–490, https://doi.org/10.1016/j.ijhydene.2024.04.155.
[19] I. Belkoufa, B. Misski, A. Alaoui-Belghiti, M. Mouyane, D. Houivet, S. Laasri, et al., Role of Mg, Ca, and Mo in $NaBH_4$ systems for hydrogen storage applications: ab initio study, Comput. Mater. Sci. 242 (2024) 113090, https://doi.org/10.1016/j.commatsci.2024.113090.
[20] I. Belkoufa, A. Assila, A. Alaoui-Belghiti, S. Laasri, E.K. Hlil, A. Hajjaji, Strain matters: enhancing the hydrogenation properties of Mg_2CoH_5 through multiaxial approaches, Int. J. Hydrogen Energy 105 (2025) 1114–1122, https://doi.org/10.1016/j.ijhydene.2025.01.353.
[21] A. Assila, I. Belkoufa, S. Sebbahi, A. Alaoui-Belghiti, E. Hlil, M. Tlemçani, et al., The role of Al substitution in Na_3AlH_6 hydrides: structural and thermodynamic insights for hydrogen storage technologies, J. Power Sources 634 (2025) 236502, https://doi.org/10.1016/j.jpowsour.2025.236502.
[22] M. Dornheim, S. Doppiu, G. Barkhordarian, U. Boesenberg, T. Klassen, O. Gutfleisch, et al., Hydrogen storage in magnesium-based hydrides and hydride composites, Scr. Mater. 56 (2007) 841–846, https://doi.org/10.1016/j.scriptamat.2007.01.003.
[23] H. Yang, H. Yuan, J. Ji, H. Sun, Z. Zhou, Y. Zhang, Characteristics of $Mg_2Ni_{0.75}M_{0.25}$ (M=Ti, Cr, Mn, Fe, Co, Ni, Cu and Zn) alloys after surface treatment, J. Alloys Compd. 330–332 (2002) 640–644, https://doi.org/10.1016/S0925-8388(01)01535-3.
[24] A. Gasiorowski, W. Iwasieczko, D. Skoryna, H. Drulis, M. Jurczyk, Hydriding properties of nanocrystalline $Mg_{2-x}M_xNi$ alloys synthesized by mechanical alloying

(M=Mn, Al), J. Alloys Compd. 364 (2004) 283–288, https://doi.org/10.1016/S0925-8388(03)00544-9.
[25] G. Liang, J. Huot, S. Boily, A. Van Neste, R. Schulz, Hydrogen storage properties of nanocrystalline $Mg_{1.9}Ti_{0.1}Ni$ made by mechanical alloying, J. Alloys Compd. 282 (1999) 286–290, https://doi.org/10.1016/S0925-8388(98)00853-6.
[26] Q. Li, Q. Lin, K.C. Chou, L.J. Jiang, F. Zhan, Hydriding kinetics of the $La_{1.5}Ni_{0.5}Mg_{17}$–H system prepared by hydriding combustion synthesis, Intermetallics 12 (2004) 1293–1298, https://doi.org/10.1016/j.intermet.2004.03.024.
[27] W.P. Kalisvaart, C.T. Harrower, J. Haagsma, B. Zahiri, E.J. Luber, C. Ophus, et al., Hydrogen storage in binary and ternary Mg-based alloys: a comprehensive experimental study, Int. J. Hydrogen Energy 35 (2010) 2091–2103, https://doi.org/10.1016/j.ijhydene.2009.12.013.
[28] C. Fan, X. Ju, C. Wan, Local and crystal structure of Mg1.9Al0.1Ni hydrogen storage alloys during hydrogen absorption–desorption cycling, Int. J. Hydrogen Energy 35 (2010) 8044–8048, https://doi.org/10.1016/j.ijhydene.2010.02.117.
[29] M.J. van Setten, G.A. de Wijs, G. Brocks, *Ab initio* study of the effects of transition metal doping of Mg_2NiH_4, Phys. Rev. B 76 (2007) 075125, https://doi.org/10.1103/PhysRevB.76.075125.
[30] H. Ding, S. Zhang, Y. Zhang, S. Huang, P. Wang, H. Tian, Effects of nonmetal element (B, C and Si) additives in Mg_2Ni hydrogen storage alloy: a first-principles study, Int. J. Hydrogen Energy 37 (2012) 6700–6713, https://doi.org/10.1016/j.ijhydene.2012.01.026.
[31] S.J. Clark, M.D. Segall, C.J. Pickard, P.J. Hasnip, M.I.J. Probert, K. Refson, et al., First principles methods using CASTEP, Z. Kristallogr. Cryst. Mater. 220 (2005) 567–570, https://doi.org/10.1524/zkri.220.5.567.65075.
[32] M.D. Segall, P.J.D. Lindan, M.J. Probert, C.J. Pickard, P.J. Hasnip, S.J. Clark, et al., First-principles simulation: ideas, illustrations and the CASTEP code, J. Phys. Condens. Matter 14 (2002) 2717–2744, https://doi.org/10.1088/0953-8984/14/11/301.
[33] J.P. Perdew, K. Burke, M. Ernzerhof, Perdew, burke, and ernzerhof reply, Phys. Rev. Lett. 80 (1998) 891, https://doi.org/10.1103/PhysRevLett.80.891, 891.
[34] D. Vanderbilt, Soft self-consistent pseudopotentials in a generalized eigenvalue formalism, Phys. Rev. B 41 (1990) 7892–7895, https://doi.org/10.1103/PhysRevB.41.7892.
[35] L.W. Huang, First principles investigation of the substitutional doping of Mn in Mg2Ni phase and the electronic structure of Mg3MnNi2 phase, J. Alloys Compd. 509 (2011) S328–S333, https://doi.org/10.1016/j.jallcom.010.08.129.
[36] Y. Gao, H. Chen, M. Shuai, X. Zeng, S. Zhao, Density functional study on the mechanics, thermodynamics, and H diffusion mechanism of LiH, Int. J. Hydrogen Energy 54 (2024) 740–750, https://doi.org/10.1016/j.ijhydene.2023.08.330.
[37] N. Govind, M. Petersen, G. Fitzgerald, D. King-Smith, J. Andzelm, A generalized synchronous transit method for transition state location, Comput. Mater. Sci. 28 (2003) 250–258, https://doi.org/10.1016/S0927-0256(03)00111-3.
[38] H. Shao, X. Li, Effect of nanostructure and partial substitution on gas absorption and electrochemical properties in Mg_2Ni-based alloys, J. Alloys Compd. 667 (2016) 191–197, https://doi.org/10.1016/j.jallcom.2016.01.180.
[39] Zolliker, et al., Structural studies of the hydrogen storage material magnesium nickel hydride (Mg_2NiH_4). 2. Monoclinic low-temperature structure |, Inorg. Chem. 25 (1986) 3590–3593, https://doi.org/10.1021/ic00240a012.
[40] Y. Zeng, K. Fan, X. Li, B. Xu, X. Gao, L. Meng, First-principles studies of the structures and properties of Al- and Ag-substituted Mg2Ni alloys and their hydrides, Int. J. Hydrogen Energy 35 (2010) 10349–10358, https://doi.org/10.1016/j.ijhydene.2010.07.131.
[41] JjJr Reilly, RhJr Wiswall, Reaction of hydrogen with alloys of magnesium and nickel and the formation of Mg_2NiH_4, Inorg. Chem. 7 (1968) 2254–2256, https://doi.org/10.1021/ic50069a016.
[42] X. Hou, H. Kou, T. Zhang, R. Hu, J. Li, X. Xue, First-principles studies on the structures and properties of Ti- and Zn-substituted Mg_2Ni hydrogen storage alloys and their hydrides, Mater. Sci. Forum 743–744 (2013) 44–52, https://doi.org/10.4028/www.scientific.net/MSF.743-744.44.
[43] B. Liu, S. Guo, Z. Hou, C. Li, X. Mu, L. Xu, et al., First-principles calculations of the crystal structure, electronic structure, and thermodynamic stability of Si-doped Mg_2Ni and Mg_2NiH_4, J. Phys. Chem. Solid. 181 (2023) 111545, https://doi.org/10.1016/j.jpcs.2023.111545.
[44] T. Hirata, Pressure DSC study of the hydrogenation and dehydrogenation of some intermetallic compounds Mg_2Ni, Int. J. Hydrogen Energy 9 (1984) 855–859, https://doi.org/10.1016/0360-3199(84)90142-3.
[45] A. Assila, M. Rkhis, A. Alaoui-Belghiti, S. Laasri, E.K. Hlil, Y. Boughaleb, et al., Feeling the strain: enhancing the thermodynamics characteristics of magnesium nickel hydride Mg_2NiH_4 for hydrogen storage applications through strain engineering, Int. J. Hydrogen Energy 67 (2024) 651–657, https://doi.org/10.1016/j.ijhydene.2024.04.159.
[46] M. Rkhis, S. Laasri, S. Touhtouh, F. Belhora, E.K. Hlil, K. Zaidat, et al., Recent advances in magnesium hydride for solid-state hydrogen storage by mechanical treatment: a DFT study, Int. J. Hydrogen Energy 48 (2023) 35650–35660, https://doi.org/10.1016/j.ijhydene.2023.05.267.
[47] H. Benzidi, M. Lakhal, M. Abdellaoui, M. Garara, A. Benyoussef, A. El Kenz, et al., Improved thermodynamic properties of doped $LiBH_4$ for hydrogen storage: first-principal calculation, Int. J. Hydrogen Energy 44 (2019) 16793–16802, https://doi.org/10.1016/j.ijhydene.2019.04.241.
[48] M. Garara, H. Benzidi, M. Abdellaoui, M. Lakhal, A. El Kenz, A. Benyoussef, et al., Hydrogen storage properties of perovskite-type $MgCoH_3$ under strain effect, Mater. Chem. Phys. 254 (2020) 123417, https://doi.org/10.1016/j.matchemphys.2020.123417.
[49] A. Baran, M. Polański, Magnesium-based materials for hydrogen storage—a scope review, Materials 13 (2020) 3993, https://doi.org/10.3390/ma13183993.
[50] L. Ren, Y. Li, N. Zhang, Z. Li, X. Lin, W. Zhu, et al., Nanostructuring of Mg-based hydrogen storage materials: recent advances for promoting key applications, Nano-Micro Lett. 15 (2023) 93, https://doi.org/10.1007/s40820-023-01041-5.
[51] M. Erika, Dematteis et al. Reactive hydride composite of Mg_2NiH_4 with borohydrides eutectic mixtures, Crystals 8 (2018) 90, https://doi.org/10.3390/cryst8020090.
[52] M. Rkhis, S. Laasri, S. Touhtouh, E.K. Hlil, A. Hajjaji, Tailoring the electrochemical performance of olivine phosphate cathode materials for Li-ion batteries by strain engineering: computational experiments, ACS Appl. Energy Mater. 6 (2023) 7074–7082, https://doi.org/10.1021/acsaem.3c00711.
[53] U. Häussermann, H. Blomqvist, D. Noréus, Bonding and stability of the hydrogen storage material Mg_2NiH_4, Inorg. Chem. 41 (2002) 3684–3692, https://doi.org/10.1021/ic0201046.
[54] X.J. Hou, H.C. Kou, T.B. Zhang, R. Hu, J.S. Li, X.Y. Xue, First-principles studies on the structures and properties of Ti- and Zn-substituted Mg_2Ni hydrogen storage alloys and their hydrides, MSF 743–744 (2013) 44–52, https://doi.org/10.4028/www.scientific.net/MSF.743-744.44.
[55] W.R. Myers, L.-W. Wang, T.J. Richardson, M.D. Rubin, Calculation of thermodynamic, electronic, and optical properties of monoclinic Mg_2NiH_4, J. Appl. Phys. 91 (2002) 4879–4885, https://doi.org/10.1063/1.1454206.
[56] X. Zhang, Z. Lou, M. Gao, H. Pan, Y. Liu, Metal hydrides for advanced hydrogen/lithium storage and ionic conduction applications, Acc. Mater. Res. 5 (2024) 371–384, https://doi.org/10.1021/accountsmr.3c00267.
[57] E. Fukushi, F. Mori, K. Munefusa, T. Harada, H. Oguchi, Epitaxial thin film growth of perovskite hydrides $MLiH_3$ (M : Sr, Ba) for the study of intrinsic hydride-ion conduction, ACS Appl. Energy Mater. 7 (2024) 2810–2815, https://doi.org/10.1021/acsaem.3c03188.
[58] T.-T. Le, M. Abbas, D.M. Dreistadt, T. Klassen, C. Pistidda, Ionic conductivity in complex hydrides for energy storage applications: a comprehensive review, Chem. Eng. J. 473 (2023) 145315, https://doi.org/10.1016/j.cej.2023.145315.
[59] H.P. Rodenburg, A. Mutschke, L. Ngamwongwan, V. Gulino, V. Kyriakou, N. Kunkel, et al., Mixed hydride-electronic conductivity in Rb2CaH4 and Cs2CaH4, Solid State Ionics 403 (2023) 116384, https://doi.org/10.1016/j.ssi.2023.116384.
[60] J. Čermák, L. Král, B. David, Hydrogen diffusion in Mg_2NiH_4 intermetallic compound, Intermetallics 16 (2008) 508–517, https://doi.org/10.1016/j.intermet.2007.12.010.
[61] New structure results for hydrides and deuterides of the hydrogen storage material Mg_2Ni - ScienceDirect n.d. https://www.sciencedirect.com/science/article/abs/pii/0022508880900740. (Accessed 18 January 2024).
[62] J.L. Soubeyroux, D. Fruchart, A. Mikou, M. Pezat, B. Darriet, Etude structurale du systeme H_2: III —La variete monoclinique de Mg_2NiH_4, Mater. Res. Bull. 19 (1984) 1119–1128, https://doi.org/10.1016/0025-5408(84)90061-8.
[63] A. Assila, I. Belkoufa, S. Sebbahi, A. Alaoui-Belghiti, S. Laasri, E.K. Hlil, M. Tlemçani, A. Hajjaji, Strain engineering of $LiFePO_4$ cathodes: effects on voltage, energy density, and electronic structure for lithium-ion batteries 125 (2025) 37–47, https://doi.org/10.1016/j.ijhydene.2025.04.075.
[64] A. Assila, I. Belkoufa, M. Rkhis, A. Alaoui-Belghiti, S. Laasri, E.K. Hlil, A. Hajjaji, Unlocking the hydrogen storage characteristics of MgH_2 hydrides: investigating the impact of mechanical strain and substitutions, J. Energy Stor. 122 (2025) 116708, https://doi.org/10.1016/j.est.2025.116708.